Side-hole to anti-hole conversion in time-resolved spectral hole burning of ruby: Long-lived spectral holes due to ground state level population storage

Riesen, Hans; Hayward, Brendan F.; Szabo, Alexander

Publisher's version / Version de l'éditeur:
https://doi.org/10.1016/j.jlumin.2007.03.015
Journal of Luminescence, 127, 2, pp. 655-664, 2007

Side-hole to anti-hole conversion in time-resolved spectral hole-burning of ruby: long lived spectral holes due to ground state level population storage.

Hans Riesen[a*], Brendan F. Hayward[a], Alex Szabo[b]

[a]*School of Physical, Environmental and Mathematical Sciences, The University of New South Wales, ADFA, Northcott Drive, Canberra, ACT 2600, Australia*
[b]*Institute for Microstructural Sciences, National Research Council of Canada 1200 Montreal Road, Ottawa, Ontario K1A 0R6, Canada*

Abstract

We report time-resolved transient spectral hole-burning of Verneuil-grown 20 ppm and ca. 1 ppm ruby ($Al_2O_3:Cr^{3+}$) in zero field and low magnetic fields B||*c* at 4 K. The hole-burning spectroscopy of the 20 ppm sample implies relatively rapid cross-relaxation in the $^4A_2$ ground state on the ~1 ms timescale both in zero field and in low magnetic fields, B||*c* up to 0.2 T. In the 1ppm sample, side-hole to anti-hole conversion is observed both in zero field and in low magnetic fields. This conversion is caused by population storage in $^4A_2$ ground state levels. Spin-lattice relaxation, on the 200 ms timescale, is directly observed from the time dependence of the resonant hole and anti-holes in B||*c*, consistent with a very low cross-relaxation rate. However, in zero field cross-relaxation in the $^4A_2$ ground state is still a significant relaxation mechanism for the 1 ppm sample resulting in a hole decay in ~50 ms.

1. Introduction

Ruby is of great historical significance in the development of the spectroscopy of impurity ions in insulators. As early as 1867-1868 Becquerel reported luminescence by the so-called R-lines ($^2E \rightarrow {}^4A_2$ transitions) [1]. In 1958 Sugano and Tanabe published their major theoretical treatise of the absorption spectra of chromium(III) in ruby, a cornerstone in the development of crystal/ligand field theory [2]. The ruby R-lines were then employed in the first successful demonstration of laser action by Maiman at Hughes Aircraft Laboratories in 1960 [3]. In other milestones, Szabo published the first observation of laser-based fluorescence line narrowing [4] and transient spectral hole-burning in a solid [5]. In the latter work on 0.03 wt % ruby, Szabo observed that optical saturation also occurred for ions that were not resonant with the laser radiation and assigned this effect to cross-relaxation in the $^4A_2$ ground state. This work was followed up and refined in a series of detailed investigations [6-10, and references therein]. Excitation energy transfer mechanisms and properties in ruby were also extensively investigated [11]. In another significant development, Macfarlane *et al* observed photon-echoes in the superhyperfine limit in 14 ppm ruby [12]. Finally, in a recent paper Bigelow *et al* purported the observation of ultraslow light propagation (group velocity of ca. 57 m/s) in ruby at room temperature [13]. However, other researchers have shown that these latter observations can be

interpreted by using a saturable absorber model without the need for group velocity reduction [14].

We have recently observed [15] conversion of side-holes to anti-holes in time-resolved transient spectral hole-burning experiments in low magnetic fields B||*c* in the chromium(III) R_1-line, $2\bar{A}\,(^2E) \leftarrow 2\bar{A}\,(^4A_2)$ of emerald, $Be_3Al_2Si_6O_{18}$:Cr(III) (0.0017 wt %), in the temperature range of 3-12 K. Anti-holes occur due to population storage in $^4A_2$ ground state Zeeman levels; this population then decays only by spin-lattice relaxation in the ground state because cross-relaxation is not effective in 0.0017% emerald.

The question then arises why this effect has not yet been reported for ruby, being an archetypal material in the spectroscopy of impurity ions in insulators. In particular, it is well documented that the spin-lattice relaxation time in ruby is about 200 ms at 4 K, and hence relatively long-lived spectral holes/anti-holes can be expected. The present article addresses this question and demonstrates that, indeed, side-hole to anti-hole conversion is also observed in ruby, but a very low chromium(III) concentration of 1 ppm is required. Moreover, even in a 1 ppm sample cross-relaxation between $^4A_2$ ground state levels is only fully eliminated upon the application of low magnetic fields B||*c*.

2. Experiment

Verneuil-grown boules of corundum crystals (Al_2O_3 nominal <1 ppm Cr(III)) and 20 ppm ruby (Djeva Ruby No 1006) were obtained from Hrand Djevahirdjian SA, Monthey, Switzerland. Samples were cut and polished parallel and perpendicular to the crystal *c*-axis with diamond-impregnated tools. Crystal thicknesses of 6.8 mm and 8.8 mm were used for the 20 ppm and <1ppm crystals, respectively. From absorption and luminescence experiments we estimate that the corundum crystal contained about 1 ppm chromium(III). The cut and polished samples were embedded using Cry-con grease on the cold finger of a closed-cycle cryostat (CCR) (Janis/Sumitomo SHI-4.5). The inhomogenous line width of the $R_1(\pm 3/2)$ transition was about 5.2 GHz for both samples. This is about 4 times wider than inhomogeneous widths observed in Czochralski grown crystals. The peak absorbance was 0.12 and ca. 0.008 for the 20 ppm and 1 ppm sample, respectively.

Excited state lifetime measurements were conducted by exciting the samples with modulated (acousto-optic modulator, Isomet 1205C-2) 532 nm light from a 10 mW Nd:YAG laser and observing the R_1-luminescence line through a Spex 1402 monochromator equipped with 1200 grooves/mm holographic gratings. The signal was measured by a photomultiplier (EMI 9785B), preamplified (Femto DLPCA-200 current-voltage preamplifier) and accumulated on a digital oscilloscope (LeCroy Wavesurfer 422).

The instrumental set-up for the transient spectral hole-burning experiments is described in detail elsewhere [15]. In brief, spectral holes were burnt and readout by a diode laser (Hitachi 6738MG, 35 mW, line-width ca. 20 MHz as measured by a spectrum analyser with 300 MHz free spectral range) mounted in a thermoelectric mount (Thorlabs TCLDM9), driven by Thorlabs TEC2000 temperature and LDC500 current controllers. The laser light was passed through an external optical diode (Faraday isolator, EOT LD38I670), amplitude-modulated by an acousto-optic modulator (Isomet 1205C-2), and after passing through an aperture and a linear polarizer (either polaroid film or Glan-Taylor calcite polarizer) focussed on the sample using a 200 mm lens. The transmitted laser light was collimated and focussed

by a 75 mm and a 200 mm lens and detected by a photodiode (Thorlabs PDA55). The signal was processed by a digital storage oscilloscope (Le Croy Wavesurfer 422) and averaged waveforms (typically 512 averages in 11-bit enhanced resolution mode) were transferred to a PC.

The sample was only exposed to laser light during the burn and readout periods. A (master) pulse generator created the burn gate (ca. 200 μs) for the RF driver of the acousto-optic modulator. The master triggered a second pulse generator (Slave 1), providing a delayed readout gate. Finally, Slave 1 triggered a waveform generator (Stanford Research Systems SRS DS345) that generated a synchronous modulation of the injection current of the diode laser by a triangular ramp, and thus a triangular modulation of the laser frequency. Ramp frequencies of 2500 Hz were used in the present experiments and the burn-read cycle was repeated at a rate of ca. 1 Hz. In comparison with the burn pulse (ca. 0.3 mW laser power), the readout light level was reduced by a factor of ca. 50.

The transverse magnetic field was generated by Helmholtz coils, arranged externally to the CCR. The coils provided a uniform magnetic field with a current dependence of 1.83 mT/A. Two power supplies (Hewlett Packard 6269 B) in series provided a current of up to 9 A at 80 V, yielding a maximum magnetic flux density B of 16 mT. The dependence of the magnetic field strength on the current was calibrated with a Hall probe. The magnetic field was fairly homogeneous, varying less than 1% within the sample volume. The crystal *c*-axis was aligned with the direction of the external magnetic field using crossed polarisers, facilitating an alignment within <2°.

For fields of 0.2 T two permanent magnets of 25 mm diameter were directly mounted on the sample holder of the closed-cycle cryostat in "Helmholtz" configuration.

3. Results and Discussion

Fig. 1 shows σ-polarized transient hole-burning spectra at 4 K for a 20 ppm ruby crystal in zero field and with an applied external field of B||*c*=15 mT. The laser was in resonance with the $R_1(\pm 3/2)$ line ($\overline{E}$ (^{2}E)← $2\overline{A}$ ($^4A_2$)), and the side-hole observed at -11.3 GHz in zero field is due to the $R_1(\pm 1/2)$ transition ($\overline{E}$ (^{2}E)← $\overline{E}$ ($^4A_2$)). The spectra of Fig. 1 were obtained by burning the hole (laser kept at constant current/frequency) for 66 ms followed by a readout period of 0.4 ms, basically rendering a "steady state" experiment. The hole-burning spectra were calculated by $\Delta A=\log_{10}(I_{nb}/I_b)$ where I_{nb} and I_b are the transmitted laser intensities without and with a burn pulse, respectively. The absorbance A at the peak maximum and the inhomogeneous width of the $R_1(\pm 3/2)$ line were about 0.12 and 5.2 GHz, respectively.

In a low magnetic field B||*c* the two spin doublet ±3/2 ($2\overline{A}$) and ±1/2 ($\overline{E}$) of the $^4A_2$ ground state, and the $\overline{E}$(^{2}E) doublet are split by $3g_{gs}\mu_B B||c$, $g_{gs}\mu_B B||c$ and $g_{ex}\mu_B B||c$, respectively. Using the trigonal selection rules for σ-polarized R-lines, side-holes are expected in B||*c* at the energies given in Table 1. Fig. 2 depicts the energy level diagram applicable to the hole-burning experiments in low magnetic fields B||*c*.

The resonant hole-width as observed in Fig. 1 is about 110 MHz, instrumentally limited by the bandwidth of the laser controller modulation circuit and the photodetector used in the experiment, and the two pairs of side-holes at –zf±319 MHz and –zf±417 MHz are not resolved in this spectrum but show up as one pair of broadened holes at ca. –zf±370 MHz in good agreement with the average. A deconvolution of these side-holes yields values of ±316 MHz and ±416 MHz in excellent agreement with the prediction based on literature g-factors (see Table 1).

Fig. 1 shows that the absorbance of the $R_1(\pm 3/2)$-line drops not only at the resonant hole, but also across the entire inhomogeneous width of this transition. In contrast, the absorbance of the $R_1(\pm 1/2)$-line increases over the entire inhomogeneous width (with the exception of the side-hole). This behaviour was observed in the early work by Szabo *et al* [5-7] and was assigned to cross-relaxation in the $^4A_2$ ground state between resonant and non-resonant ions.

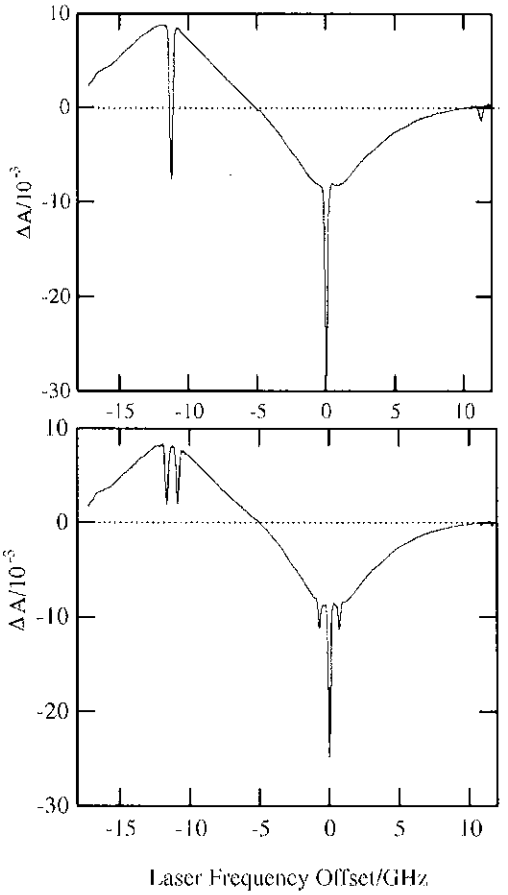

Fig. 1: Quasi steady-state σ-polarized, transient hole-burning spectra for the $R_1(\pm 3/2)$ line of a 20 ppm ruby crystal at 4 K in a) zero field and b) a field of B||*c*=15 mT. ΔA is the change in absorbance (optical density).

Table 1: Predicted (literature g-values used) and observed energies of side-holes relative to the resonant hole with B||c. The terms g_{gs}(=1.985) and g_{ex} (=2.45) denote g||($^4A_2$) and g||($\overline{E}$ (^{2}E)), respectively.

Side-holes in B||*c*	Side-holes in B||*c*=15 mT	Observed in B||*c*=15 mT
$\pm \mu_B B\|\|c(3g_{gs}-g_{ex})$	±736 MHz	±735 MHz
$-zf\pm \mu_B B\|\|c(2g_{gs}-g_{ex})$	-zf±319 MHz	-11.3±316 MHz
$-zf\pm \mu_B B\|\|c(g_{gs})$	-zf±417 MHz	-11.3±416 MHz

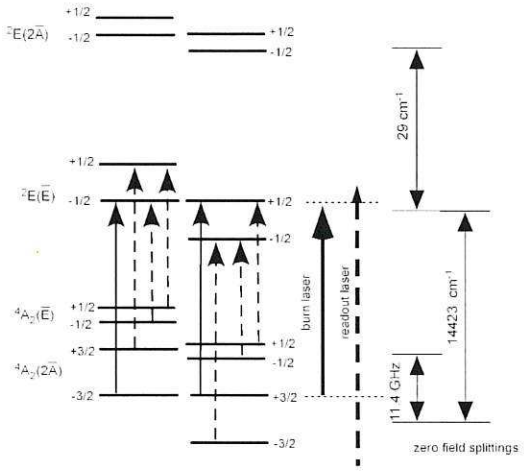

Fig. 2: Schematic six-level diagram for the analysis of hole/side-hole/anti-hole patterns in ruby in σ polarization and in low magnetic fields B||*c*. The zero field splittings are indicated on the right hand side. The dashed arrows on the left hand side indicate the transitions yielding side/anti-holes.

Fig. 1 confirms that cross-relaxation between the optically resonant ions and the non-resonant ions in the zero-field split $^4A_2$ ground state is highly effective. This leads to a decrease and increase of the absorption of the $R_1(\pm 3/2)$ and $R_1(\pm 1/2)$ transitions, respectively, over their entire inhomogeneous width as is schematically illustrated in Fig. 3. This is because the spin-lattice relaxation rate is relatively slow (ca. 5 s^{-1} at 4 K) compared to the cross-relaxation rate. Hence the population of non-resonant ions in the ±1/2 spin-doublet increases and the population of the non-resonant ions in the ±3/2 spin-doublet decreases with increasing pump power. Similar effects have been reported by Jessop and Szabo in some early work on 0.03 % ruby [7]. In this work the inhomogeneous linewidth was 1.4 GHz (Czochralski grown rubies) whereas the Verneuil grown rubies of the present work had an inhomogeneous linewidth of 5.2 GHz and hence a substantially lower optical density A at the laser frequency. This in turn leads to lower changes in absorbance ΔA.

Fig. 4 shows time-resolved transient hole-burning spectra for 20 ppm ruby in the ($\bar{E}(^2E) \leftarrow 2\bar{A}(^4A_2)$) transition(s) in zero field and in a low magnetic field B||*c*. The side-holes appear at $\pm \mu_B B||c(3g_{gs}-g_{ex})$ (see Table 1). This figure also illustrates the narrowing of the resonant hole upon the application of a small magnetic field. The zero field data shows a hole-width of ca. 80 MHz whereas the resonant hole in B||*c*=11.2 mT is ca 38 MHz. The laser line-width is about 20 MHz, and thus the hole-width is basically reflecting the instrumental resolution. Integrated hole areas, as obtained from data such as that illustrated in Fig. 4, are summarized in Fig. 5 as a function of the delay time between the burn pulse and the probe pulse. Fig. 5 also displays data for the resonant hole area obtained in B||*c*=0.2 T. Within the experimental accuracy no variation between the 11.2 mT and the 0.2 T can be discerned. The data in Fig. 5 implies that the hole/side-hole decay is governed by the excited state lifetime and relatively fast cross-relaxation, eliminating any build up of resonant ions in the ±1/2 spin levels upon initial pumping from the ±3/2 levels.

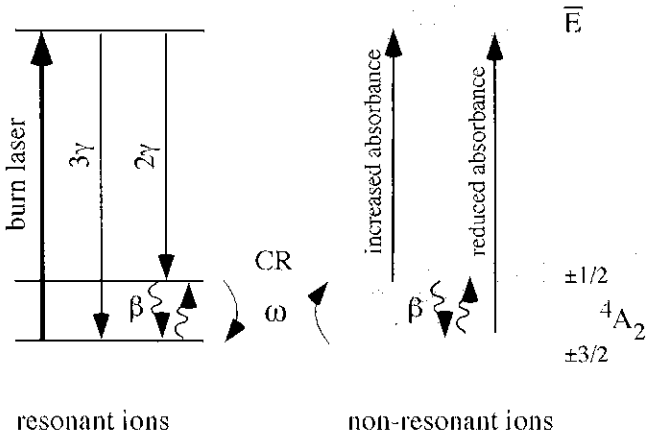

Fig. 3: Schematic diagram of the dynamical processes in the R_1 line of ruby in zero field. The excited state lifetime is $(5\gamma)^{-1}$, the spin-lattice relaxation rate between the ±1/2 and ±3/2 spin doublets is denoted by β and the cross-relaxation (CR) process between the resonant and non-resonant ions is denoted by ω.

The following set of differential equations provide a good approximation for the zero field data of Fig. 5 as follows from the three level system depicted in Fig. 3,

$$\dot{n}_1 = -\beta(n_1 - n_2) + 3\gamma n_3 - \frac{\omega'}{N}(n_1 N_2 - n_2 N_1) \tag{1}$$

$$\dot{n}_2 = -\beta(n_2 - n_1) + 2\gamma n_3 - \frac{\omega'}{N}(n_2 N_1 - n_1 N_2) \tag{2}$$

$$\dot{n}_3 = -5\gamma n_3 \tag{3}$$

where n_i indicate the population of the levels of the ions that are resonant with the laser, the upper case $N_{i,j}$ indicate the population of the levels of the ions that are *not* resonant with the laser light, N is the total population of non-resonant ions and ω' is the cross-relaxation rate for ±3/2↔±1/2. The data in Fig. 5 was obtained using short burn pulses of 190 μs and hence we use the approximation $N_1 \approx N_2 \approx \text{constant} \approx N/2$, simplifying the above equations. The solution for the hole area in the $\overline{E}(^2\text{E}) \leftarrow 2\overline{A}(^4\text{A}_2)$ transition then becomes,

$$A(t) = \frac{A_0}{2}\left\{\frac{3\alpha - 8\gamma}{2\alpha - 5\gamma}e^{-5\gamma t} + \frac{\alpha - 2\gamma}{2\alpha - 5\gamma}e^{-2\alpha t}\right\} \tag{4}$$

where $\alpha = \beta + \omega'/2$, and A_0 denotes the initial hole area after the burn pulse.
In a low magnetic field B||*c* we have to add the energy levels of the non-resonant ions to the six-level diagram of Fig. 2. After excitation by a laser pulse, the system will

return back to thermal equilibrium as described by the set of coupled differential Eqs. (5),

$$\dot{n}_i = -n_i \sum_j w_{ij} + \sum_j n_j w_{ji} - \frac{1}{N} \sum_j \omega_{ij} \left(n_i N_j - n_j N_i \right) \qquad (5)$$

where n_i denotes the population of the resonant ions of level i and w_{ij} are the transition probabilities between levels i and j, comprising non-radiative and both induced and spontaneous radiative processes and ω_{ij} describe cross-relaxation rates between resonant and non-resonant ions in $^4A_2$ ground state levels.

We have solved the set of differential Eqs. 5 for the two limiting cases of fast and negligible cross-relaxation. The experiments of the current work were conducted at 4 K. The spin lattice relaxation time for the Zeeman split $\overline{E}(^2E)$ levels was found to accurately follow the temperature dependence of an Orbach process as is given by Eq. 6 [16],

$$T_1 = 3.8 \times 10^{-9} \exp(\Delta / k_B T) \qquad (6)$$

with $\Delta = {}^2E = 29$ cm^{-1} splitting and k_B the Boltzmann constant. At 4 K the spin lattice relaxation time is ca 130 μs and is thus on the timescale of the burn pulse. Moreover, the shortest delay between burn and read laser used in the present experiments was ca. 0.2 ms. Hence the two Zeeman levels in the excited state are thermalised on the experimental timescale of the present data. Also, if we use a short laser pulse (low burn fluence) we can make the approximation that $N_1 \approx N_2 \approx N_3 \approx N_4 \approx N/4 = \text{constant}$, where N is the total population of non-resonant ions.

If spin-lattice relaxation is much slower than cross-relaxation, we can neglect the former and following set of equations is obtained when the $\Delta Ms = \pm 1$ selection rule is applied for the transitions involved in the cross-relaxation process:

$$\dot{n}_1 = 3\gamma n_5 - \frac{\omega}{4}(n_1 - n_3) \qquad (7)$$

$$\dot{n}_2 = 3\gamma n_6 - \frac{\omega}{4}(n_2 - n_4) \qquad (8)$$

$$\dot{n}_3 = 2\gamma n_5 - \frac{\omega}{4}(2n_3 - n_4 - n_1) \qquad (9)$$

$$\dot{n}_4 = 2\gamma n_6 - \frac{\omega}{4}(2n_4 - n_3 - n_2) \qquad (10)$$

$$\dot{n}_{5,6} = -5\gamma n_{5,6} \qquad (11)$$

If we burn into +3/2 and -3/2 in a field we then get following solution for the decay of the resonant hole area, A_{rh}, due to excited state deactivation and cross-relaxation

$$A_{rh}(t) =$$

$$\frac{2}{3}A_0\left\{\exp(-5\gamma t)\frac{3\omega-32\gamma}{4(\omega-10\gamma)}+\exp(-\omega t/2)\left[\frac{(\omega-8\gamma)}{4(\omega-10\gamma)}+\frac{1}{2}\cosh\left(\frac{1}{4}t\sqrt{2}\omega\right)+\frac{\sqrt{2}}{4}\sinh\left(\frac{1}{4}t\sqrt{2}\omega\right)\right]\right\} \quad (12)$$

where A_0 is the initial hole area. The side hole area, A_{sh}, as a function of time is given by:

$$A_{sh}(t) =$$

$$\frac{1}{3}A_0\left\{\exp(-5\gamma t)\frac{3\omega-32\gamma}{4(\omega-10\gamma)}+\exp(-\omega t/2)\left[\frac{(\omega-8\gamma)}{4(\omega-10\gamma)}-\frac{1}{2}\cosh\left(\frac{1}{4}t\sqrt{2}\omega\right)-\frac{\sqrt{2}}{4}\sinh\left(\frac{1}{4}t\sqrt{2}\omega\right)\right]\right\} \quad (13)$$

We note here that the cross-relaxation rate ω in Eqs. (12) and (13) is related to ω' in Eq. 4 by $\omega'=\omega/2$.

The data of Fig. 5 were globally fitted by Eqs. 4, 12 and 13. In this global fit the excited lifetime was fixed to 4.14 ms, the value we measured for the 20 ppm sample used in this work. Hence the global fit contained only the adjustable parameter ω and the initial hole area. A value of ω=1.55 (± 0.06) $\times 10^3$ s^{-1} is found, corresponding to a cross-relaxation time of ca. 1.3 ms. The data is well described up to delay times of 10 ms. However, for times longer than 10 ms the hole area in B||c=11.2 mT and 0.2 T decays slower than predicted by Eq. (12). It appears that the decay of the majority of chromium(III) centres follows Eqs. (12) and (13) with the same cross-relaxation time as in zero field but for a minority of centres the cross-relaxation time increases to ca 24 ms upon the application of a field. This observation is further discussed below.

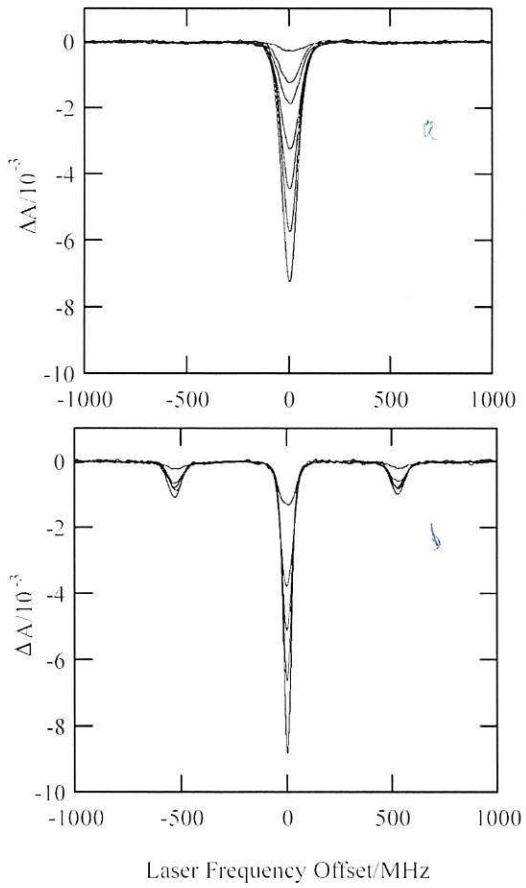

Fig. 4: Time-resolved transient spectral hole-burning in σ-polarization at 4 K in the $R_1(\pm 3/2)$ line of a 20 ppm ruby in a) zero field and b) with B||*c*=11.2 mT. Traces were obtained at burn-read pulse delays of a) 0.215 ms, 0.502 ms, 0.853 ms, 1.62 ms, 3.23 ms 4.82 ms, 9.57 ms; b) 0.21 ms, 0.36 ms, 0.852 ms, 1.41 ms, 4.78 ms (bottom to top trace).
The side-holes occur at $\pm\mu_B B||c(3g_{gs}-g_{ex})$. Width of burn pulse: 190 μs.

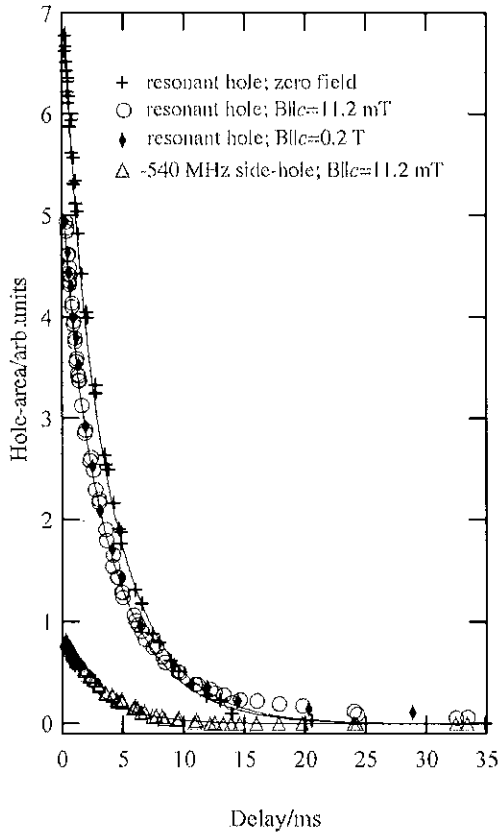

Fig. 5: Hole and side-hole decays at 4 K in σ-polarized time-resolved transient spectral hole-burning in the $R_1(\pm 3/2)$ line of a 20 ppm ruby in zero field, B||c=11.2 mT (spectra illustrated in Fig. 4) and B||c=0.2 T. The solid lines result from a global fit to Eqs. 4, 12 and 13 as discussed in the text.

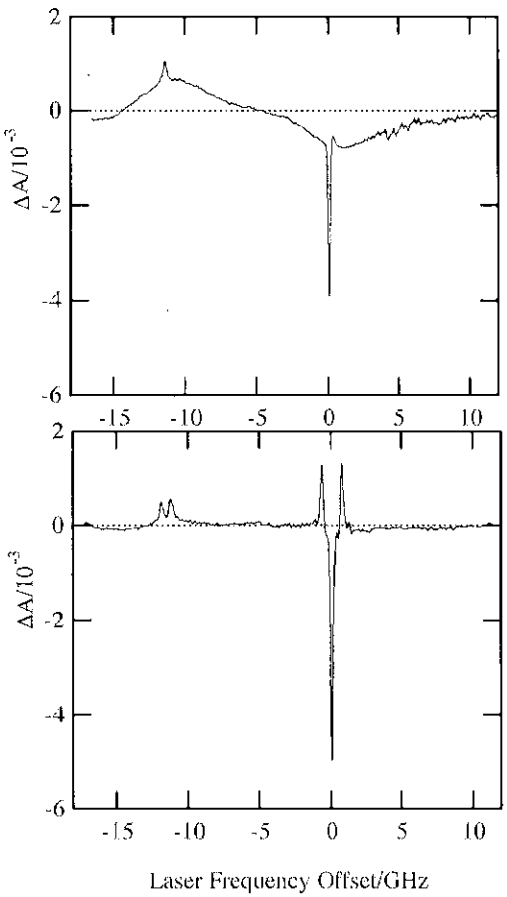

Fig. 6: Quasi steady-state σ-polarized,transient hole-burning spectra at 4 K in a) zero field and b) a field of B||*c*=15 mT for the $R_1(\pm 3/2)$ line of a 1 ppm ruby crystal.

Fig. 6 shows σ-polarized transient hole-burning spectra at 4 K for the 1 ppm ruby crystal under the same conditions as shown for the 20 ppm sample in Fig. 1. Cross-relaxation still has a significant effect in zero field, yielding an increase and decrease across the entire inhomogeneous width of the $R_1(\pm 1/2)$ and $R_1(\pm 3/2)$ line, respectively. However, the application of B||*c*=15 mT eliminates this effect.

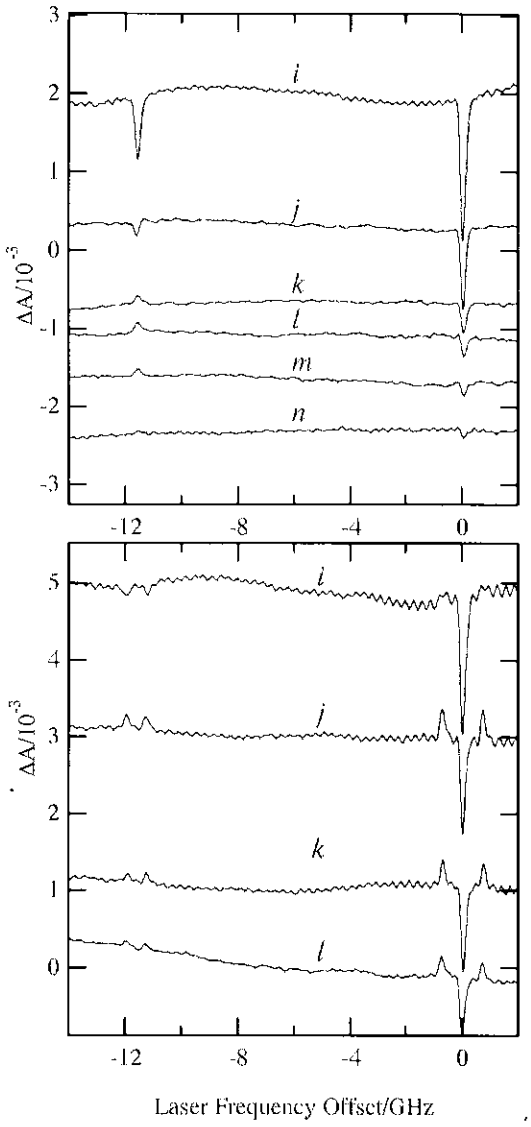

Fig. 7: Time-resolved transient spectral hole-burning in a 1 ppm ruby crystal at 4 K in σ-polarization in a) zero field and b) B||*c*=15 mT. Delays between pump and probe pulse are a) *i*=0.2 ms, *j*=4.2 ms, *k*=10.2 ms, *l*=16.2 ms, *m*=32.2 ms and *n*=65 ms and b) *i*=0.2 ms, *j*=16.2 ms, *k*=32.2 ms and *l*=65 ms and. Width of burn pulse: 1.6 ms. Traces are vertically displaced.

Fig. 7 shows time-resolved transient hole-burning spectra in zero field and in B||*c*=15 mT with various delays between the burn and readout pulse. The resonant hole is burnt into the $R_1(\pm 3/2)$-line. Side-holes/anti-holes are due to the ±1/2 level in zero field and due to all the resulting Zeeman levels of the ±3/2 and ±1/2 spin doublets in a field. The spectra in zero field show that the initial side-hole converts into an anti-hole as time progresses. This is due to a build up of population in the ±1/2 ground state level upon burning into the $R_1(\pm 3/2)$-line. The same happens in a magnetic field with the Zeeman split levels but on a much longer timescale. This confirms that in zero field there is an extra relaxation mechanism which, on the basis of Fig. 6, can clearly

be identified as cross-relaxation between resonant and non-resonant ions. The much longer timescale on which the hole/anti-holes decay in a magnetic field implies that cross-relaxation is more or less eliminated in the 1 ppm sample by the application of a very low external magnetic field B||c and the decay at longer times is governed by the spin-lattice relaxation time in the ground state. (Please note that the absorbance increase and decrease due to cross-relaxation across the inhomogeneously broadened transition is not obvious in the zero field data of Fig. 7 since a relatively short burn pulse was used.)

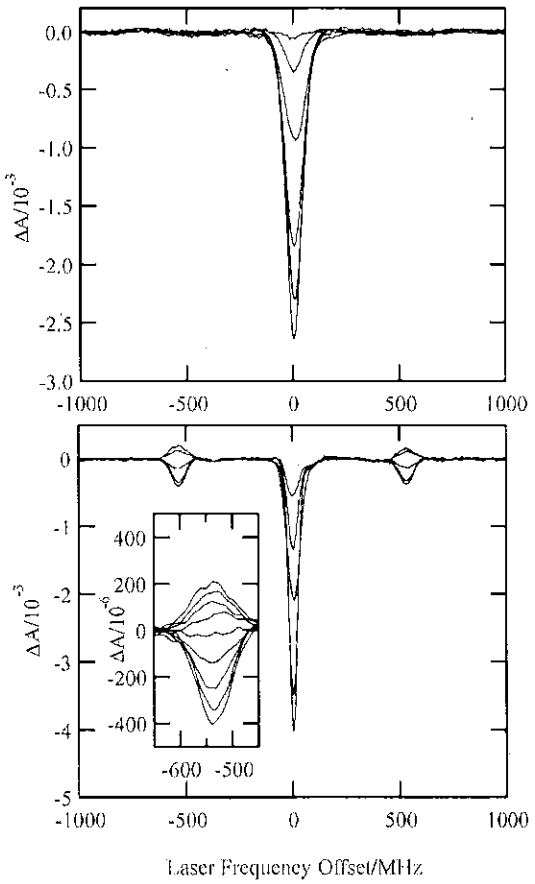

Fig. 8: Time-resolved transient spectral hole-burning in σ-polarization at 4 K in the $R_1(\pm 3/2)$ line of a 1 ppm ruby with B||c=11.2 mT. Traces were obtained at delays of a) 0.228 ms, 0.556 ms, 1.155 ms, 3.3 ms, 12.5 ms, 95 ms; b) 0.223 ms, 0.596 ms, 1.852 ms, 18.8 ms, 134 ms (from bottom to top). The side-holes/anti-holes occur at $\pm\mu_B B||c(3g_{gs}-g_{ex})$. The insert shows, in detail, the evolution of the side-hole at –540 MHz into an anti-hole with progressing delay times (from bottom to top trace) of 0.223 ms, 0.596 ms, 1.15 ms, 1.85 ms, 3.31 ms, 5.42 ms, 6.60 ms, 12.4 ms, 18.4 ms. Width of burn pulse: 190 μs.

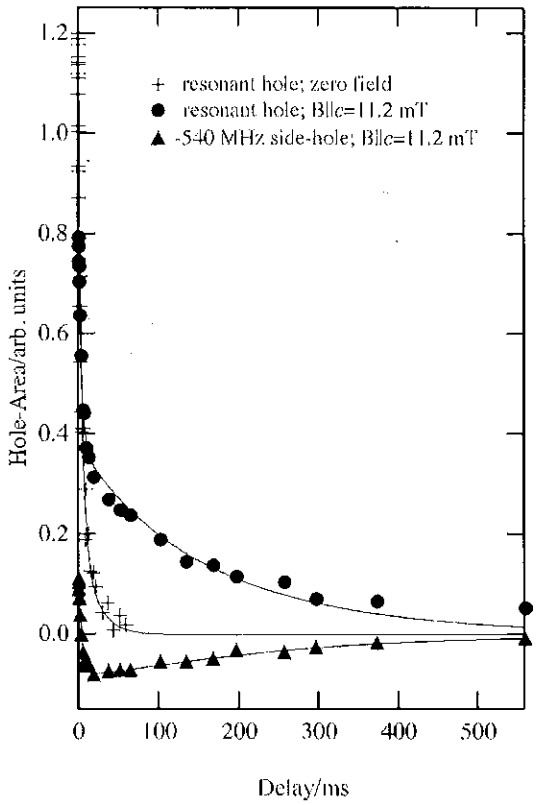

Fig. 9: Hole and side-hole/anti-hole decay at 4 K in σ-polarized time-resolved transient spectral hole-burning in the $R_1(\pm 3/2)$ line of 1 ppm ruby in zero field and B||c=11.2 mT. The solid lines are fits to Eqs. 4, and 19 and 20 for the hole in zero field and the resonant hole and the side-hole at -540 MHz in a field, respectively.

In Fig. 8 transient hole-burning spectra in zero field and in B||c=11.2 mT in vicinity of the resonant hole in the $R_1(\pm 3/2)$ line are shown in more detail for a range of delay times. The B||c=11.2 mT data illustrates the time evolution of the side-holes into anti-holes due to a population build-up in ground state Zeeman levels; for example, if the laser is in resonance with the $R_1(-3/2)$ line of a particular subset of ions, these ions can end up, with a probability given by the transition dipole moments, in the corresponding +3/2 level, yielding an increase of the population of this level and hence an increase of the absorption (anti-hole). Since cross-relaxation is no longer effective for the 1 ppm crystal in a low magnetic field B||c, the only way of subsequently thermalising the system is by spin-lattice relaxation.
The time-dependence of the integrated hole-areas, obtained from data as illustrated in Fig. 8, is summarized in Fig. 9. Figs. 10 and 11 show data obtained in a very small magnetic field of B||c=3.7 mT. Within the experimental accuracy, the integrated hole areas show the same behaviour as a function of time as the B||c=11.2 mT data i.e. a field of B||c=3.7 mT eliminates cross-relaxation as effectively as 11.2 mT.

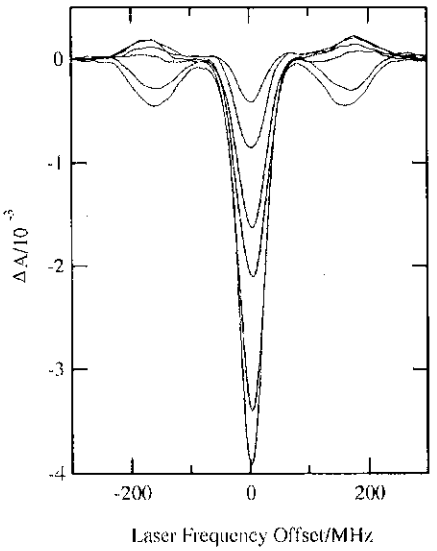

Fig. 10: Time-resolved transient spectral hole-burning in σ-polarization at 4 K in the $R_1(\pm 3/2)$ line of a 1 ppm ruby with B||c=3.7 mT. Traces were obtained at delays of 0.266 ms, 0.864 ms, 4.86 ms, 11.51 ms, 107.6 ms, 250 ms (from bottom to top). The side-holes/anti-holes occur at $\pm\mu_B B||c(3g_{gs}-g_{ex})=\pm 180$ MHz. Width of burn pulse: 190 μs.

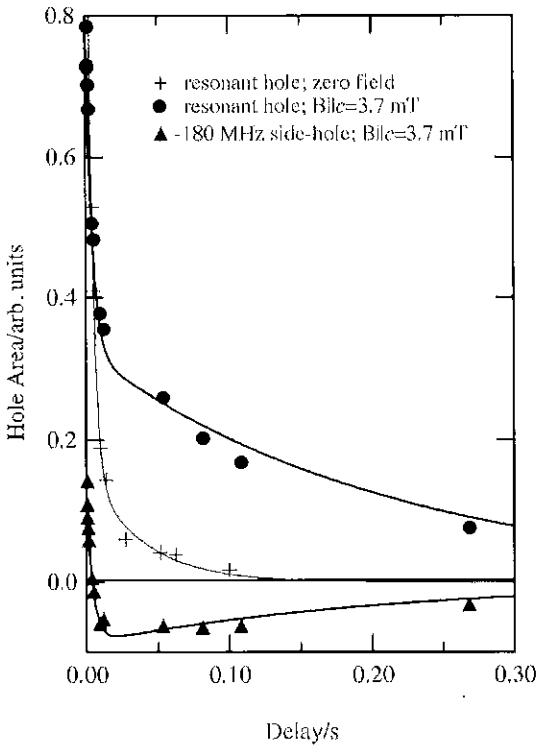

Fig. 11: Hole and side-hole decays at 4 K in time-resolved transient spectral hole-burning in the $R_1(\pm 3/2)$ line of a 1 ppm ruby in zero field and B||c=3.7 mT. The solid lines are fits to Eqs. 4, 19 and 20.

Cross-relaxation can be neglected thus be neglected and we use the selection rules $\Delta Ms=\pm 2$ and $\Delta Ms=\pm 1$ apply for the spin-lattice relaxation process. Also, one can show theoretically that the spin flip $+1/2 \leftrightarrow -1/2$ is extremely slow and this has been confirmed experimentally in high magnetic fields [17]. We assume that the rates for the allowed transitions are the same (β). Following set of differential equations then describes the six level system. Again, we assume that the spin-lattice relaxation in the excited state is very fast (see above).

$$\dot{n}_1 = -2\beta n_1 + (n_3 + n_4)\beta + 3\gamma n_5 \qquad (14)$$

$$\dot{n}_2 = -2\beta n_2 + (n_3 + n_4)\beta + 3\gamma n_6 \qquad (15)$$

$$\dot{n}_3 = -2\beta n_3 + (n_1 + n_2)\beta + 2\gamma n_5 \qquad (16)$$

$$\dot{n}_4 = -2\beta n_4 + (n_1 + n_2)\beta + 2\gamma n_6 \qquad (17)$$

$$\dot{n}_{5,6} = -5\gamma n_{5,6} \qquad (18)$$

Solving this set of differential equations leads to following time dependence for the resonant hole area A_{rh} and the side hole area A_{sh} (-3/2 for +3/2 or +3/2 for -3/2) if initially the +3/2 or -3/2 level are depleted by a short laser pulse.

$$A_{rh}(t) = \frac{2}{3}A_0\left[\frac{1}{2}\exp(-2\beta t) + \frac{\beta-\gamma}{4\beta-5\gamma}\exp(-4\beta t) + \frac{3\beta-4\gamma}{4\beta-5\gamma}\exp(-5\gamma t)\right] \qquad (19)$$

$$A_{sh}(t) = \frac{1}{3}A_0\left[\frac{\beta-\gamma}{4\beta-5\gamma}\exp(-4\beta t) + \frac{3\beta-4\gamma}{4\beta-5\gamma}\exp(-5\gamma t) - \frac{1}{2}\exp(-2\beta t)\right] \qquad (20)$$

where A_0 is the initial hole area of the resonant hole.

The data of Figs. 9 and 11 are well described by Eqs. 4, 19 and 20. In the fit for the zero field data the excited lifetime was fixed at 3.75 ms. This is the 4-K excited state lifetime determined for the 1 ppm sample used in the present work. The fit yields a rate of $\alpha=25.8\ s^{-1}$. The spin-lattice relaxation time is about 200 ms at 4 K [18] and hence the cross-relaxation time in the 1 ppm sample is about 48 ms in zero field. The decrease in the zero field cross-relaxation time is due to the larger chromium(III)-chromium(III) distance R; the cross-relaxation rate between two ions is proportional to $1/R^6$ as it is based on magnetic dipole-dipole interaction. The mean R value increases from ~55 Å to ~151 Å from 20 ppm to 1ppm ruby. Hence a significant reduction of the cross-relaxation rate can be expected going from 20 ppm to 1 ppm. If we assume that the cross-relaxation rate is proportional to the expectation value $\left\langle \sum_j \frac{1}{R_{ij}^6} \right\rangle$, it is expected to be directly proportional to the chromium(III) concentration. The observed reduction is in reasonable agreement with this consideration. Table 2 summarises the observed cross-relaxation times.

The data in a magnetic field was globally fitted by Eqs. 19 and 20, with the excited state lifetime fixed, yielding a value for $\beta=2.59\ s^{-1}$. This corresponds to a spin-lattice

relaxation time $(2\beta)^{-1}$ of 193 ms for the $^4A_2$ ground state at 4 K in perfect agreement with early EPR measurements [18].

Table 2: Summary of some measured $^4A_2$ cross-relaxation times in ruby

Cr(III) concentration	Field, B‖c	cross-relaxation time
1 ppm	zero field	48 ms
1 ppm	3.7 mT	>200 ms
1 ppm	11.2 mT	>200 ms
20 ppm	zero field	1.3 ms
20 ppm	11.2 mT	1.3 ms (+24 ms minority component)
20 ppm	0.2 T	1.3 ms (+24 ms minority component)
20 ppm[a]	0.4 T	2.5 ms[a]
340 ppm	0.35 T	25 μs[b]

[a] Ref. 9; [b] Ref. 8

Cross-relaxation is virtually eliminated upon the application of a small magnetic field B‖*c* for the 1 ppm sample. This observation can be rationalized by considering the superhyperfine interaction of the ^{27}Al nuclear spins (I=5/2) with the chromium(III) electron spin system. In order to flip-flop two chromium(III) spins, they must have the same energy configuration of the surrounding aluminium's. In other words, the ca. 30 MHz EPR linewidth at 4 K is heterogeneously broadened; that is the chromium(III) frequency jitters around depending on the aluminium(III) energy configuration. To conserve energy, a direct chromium(III) spin flip-flop will only occur when the two spins are within the homogeneous linewidth of ca. 10 kHz. This process is magnetic field dependent as the superhyperfine splitting increases with increasing magnetic field. Hence in zero field it is much easier to meet the energy conservation requirement.

In the case of the 20 ppm sample at 4 K, the frequency fluctuations due to indirect chromium(III) flips at a given chromium(III) site exceed that due to aluminium nuclear spin flips, and hence again the energy conservation requirement is more easily met. These electron flip-flops will not cease upon the application of a low magnetic field and hence there is little dependence of the cross-relaxation rate in the 20 ppm sample. However, we observe that a minority of sites is subject to an increase of the cross-relaxation time from 1.3 ms to 24 ms. It is clear that the cross-relaxation rate is subject to a distribution because there are chromium(III) ions that are significantly more isolated from other centres than the average. These minority chromophores will experience a magnetic field effect similar to the 1 ppm sample. We note here that in earlier work on photon echoes in 23 ppm ruby B‖*c*>2 T were required to eliminate Cr spin-flip effects [19].

4. Conclusions

The present article shows that direct electron-spin-electron-spin interactions are governing the relaxation times in the $^4A_2$ ground state of a 20 ppm ruby sample and are still significant in a 1 ppm samples in zero field. However, in the latter case the application of a low magnetic field B‖*c* on the order of magnitude of several mT is

sufficient to eliminate the effects of cross-relaxation. As a consequence side-hole to anti-hole conversion is observed, for the first time in ruby, with increasing delay times between the burn and readout pulse and the lifetime of holes is governed by the spin-lattice relaxation time of ca. 200 ms at 4 K. Side-hole to anti-hole conversion was previously observed in 0.0017 wt % emerald. Emerald has an aluminium density about 8 times lower than ruby and hence a 0.0017 wt % emerald crystal corresponds to ca. 0.0002 wt % ruby regarding chromium(III)-chromium(III) distances for cross-relaxation. Moreover, the superhyperfine interaction is also reduced due to the larger aluminium-chromium separation. Vice versa, the 20 ppm ruby would correspond to 160 ppm emerald. We note here that no side-hole to anti-hole conversion was observed in work on 0.04 % emerald [20].

The present work shows, again, that *g*-factors and spin-lattice relaxation times can be observed directly by time-resolved transient hole-burning spectroscopy We conclude that for paramagnetic samples extremely low concentrations must be employed in order to draw valid conclusions about optical properties in zero field and low magnetic fields.

The direct spin flip time in the 20 ppm sample is about 1.3 ms; this has to be compared to the dephasing time of 15 μs for the R_1 transition at this concentration. This confirms that indirect flips of chromium(III) spins are responsible for the optical dephasing in accord with conclusions reached in previous work [9]. However, the chromium(III) flip rate is controlled by the aluminium energy configuration and its rate of change (nuclear spin flip flops) around the chromium(III) centres [8].

Acknowledgement

We like to thank Ms K. Djevahirdjian and Mr K. Blaser of Hrand Djevahirdjian SA, Monthey, Switzerland for providing us with samples of ruby/corundum.

References

[1] A.E. Becquerel, La Lumiere, ses causes et ses effets (Paris: Didot, 1867-1868) (reproduction: Microopaque. New York, N.Y.; Readex Microprint Corporation, 1968)

[2] S. Sugano, Y. Tanabe, J. Phys. Soc. Jap. 13 (1958) 880.

[3] T.H. Maiman, Nature 187 (1960) 493.

[4] A. Szabo, Phys. Rev. Lett. 27 (1971) 323–326.

[5] A. Szabo, Phys. Rev. B 11 (1975) 4512.

[6] P.E. Jessop, T. Muramoto, A. Szabo, Phys. Rev. B 21 (1980) 926.

[7] P.E. Jessop, A. Szabo, in Laser Spectroscopy V, ed. A. McKellar, T. Oka, B.P. Stoicheff, Springer-Verlag (1981) p. 408.

[8] A. Szabo, T. Muramoto, R. Kaarli, Phys. Rev. B 42 (1990) 7769.

[9] A. Szabo, R. Kaarli, Phys. Rev. B. 44 (1991) 12307.

[10] A. Szabo, J. Lumin. 56 (1993) 47.

[11] P.M. Seltzer, D.L. Huber, B.B. Barnett, W.M. Yen, Phys. Rev. B 17 (1978) 4979.

[12] (a) J. Ganem, Y.P. Wang, D. Boye, R.S. Meltzer, W.M. Yen, R.M. Macfarlane Phys. Rev. Lett. 66 (1991) 695.

(b) J. Ganem, Y.P. Wang, D. Boye, R.S. Meltzer, W.M. Yen, R. Wannemacher, R.M. Macfarlane, Phys. Rev. Lett. 66 (1991) 1649.

[13] M.S. Bigelow, N.N. Lepeshkin, R.W. Boyd, Phys. Rev. Lett. 90 (2003) 113903-1.

[14] V.S. Zapasskii, G.G. Kozlov, Opt. Spectr. 100 (2006) 419-424.
[15] B.F. Hayward, H. Riesen, Phys. Chem. Chem. Phys. 7 (2005) 2579-2586.
[16] S. Geschwind, G.E. Devlin, R.H. Cohen, S.R. Chinn, Phys. Rev. 137 (1965) A1087.
[17] A. Misu, J. Phys. Soc. Japan 44 (1978) 1161.
[18] J.C. Gill, Proc. Phys. Soc. 79 (1962) 58.
[19] A. Szabo, J. Lumin. 58 (1994) 403.
[20] H. Riesen, Chem. Phys. Lett. 382 (2003) 578.